Nanoscale

RSC Publishing

PAPER

View Article Online
View Journal | View Issue

Cite this: *Nanoscale*, 2013, **5**, 1168

Dopamine as the coating agent and carbon precursor for the fabrication of N-doped carbon coated Fe_3O_4 composites as superior lithium ion anodes†

Cheng Lei, Fei Han, Duo Li, Wen-Cui Li, Qiang Sun, Xiang-Qian Zhang and An-Hui Lu*

Received 5th October 2012
Accepted 25th November 2012

DOI: 10.1039/c2nr33043a

www.rsc.org/nanoscale

Dopamine is an excellent and flexible agent for surface coating of inorganic nanoparticles and contains unusually high concentrations of amine groups. In this study, we demonstrate that through a controlled coating of a thin layer of polydopamine on the surface of α-Fe_2O_3 in the dopamine aqueous solution, followed by subsequent carbonization, N-doped carbon-encapsulated magnetite has been synthesized and shows excellent electrochemical performance as anode material for lithium-ion batteries. Due to the strong binding affinity to iron oxide and excellent coating capability of this new carbon precursor, the conformal polydopamine derived carbon is continuous and uniform, and its thickness can be tailored. Moreover, due to the high percentage of nitrogen content in the precursor, the resulting carbon layer contains a moderate amount of N species, which can substantially improve the electrochemical performance. The composites synthesized by this facile method exhibit superior electrochemical performance, including remarkably high specific capacity (>800 mA h g^{-1} at a current of 500 mA g^{-1}), high rate capability (595 and 396 mA h g^{-1} at a current of 1000 and 2000 mA g^{-1}, respectively) and excellent cycle performance (200 cycles with 99% capacity retention), which adds to the potential as promising anodes for the application in lithium-ion batteries.

1 Introduction

Rechargeable lithium-ion batteries (LIBs) are currently being explored for high-power energy applications such as electric vehicles and smart utility grids.[1–3] Due to the low theoretical capacity (372 mA h g^{-1}) of graphitic carbon, which is the most commonly used anode material, the current LIBs are approaching limits set by the electrode materials.[4] Thus, the search for alternative anode materials has become an urgent task in building the next-generation LIBs, so as to meet the ever-growing performance demands.[5] One of the feasible candidates for anode materials is nano-sized transition-metal oxides.[6] Among them, nanostructured Fe_3O_4 has attracted considerable attention owing to its low cost, eco-friendliness, natural abundance and high capacity.[7–13] However, its practical application is still hindered by poor cyclic performance and rate capability, resulting from severe aggregation and dramatic volume change during Li^+ insertion/extraction processes.[14,15] Moreover, the low conductivity of iron oxide often further hastens the degradation process.[16] To mitigate the aggregation and large-volume variation of magnetite during discharge–charge process, and increase the electronic conductivity, strategies of coating carbon on magnetite nanoparticles have been extensively explored.[2,3,7,14,17–21] To achieve high-rate capability and high capacity using iron oxide nanoparticles coated with a carbon layer, two key issues must be considered: (i) the carbon layer should be uniform and continuous, so that it can provide rapid and continuous electronic transport and prevent the direct contact between the iron oxide and electrolyte, thus avoiding capacity fading and safety problems;[7,22,23] (ii) a carbon coating layer with optimized thickness should be developed, to ensure both elastic and good mechanical stability, as a carbon layer with appropriate thickness can buffer the dramatic volume expansion and keep the structural integrity. When the carbon layer is too thin, it is difficult to form a buffer layer which is strong enough to accommodate the tension. Even worse, the carbon layer may be intermittent in some cases especially for a one-pot method,[29,30] which may reduce the electronic conductivity of the composite. Conversely, when the carbon layer is too thick, the specific capacity of the composites may decline because of the relatively low content of iron oxides and restricted efficient ion transfer/transport.[24] Therefore, it is extremely important to control the thickness, uniformity and continuity of a carbon layer for high performance iron oxide@C composite anodes.

State Key Laboratory of Fine Chemicals, School of Chemical Engineering, Faculty of Chemical, Environmental and Biological Science and Technology, Dalian University of Technology, Dalian 116024, P.R. China. E-mail: anhuilu@dlut.edu.cn; Fax: +86-411-84986112; Tel: +86-411-84986112

† Electronic supplementary information (ESI) available. See DOI: 10.1039/c2nr33043a

Glucose has generally been used as the carbon source to fabricate carbon-coated Fe_3O_4 nanorods,[18] nanospindles,[7] nanospheres,[25] and nanowires,[26] through hydrothermal synthesis. The obtained composites present better electrochemical performances than pure Fe_3O_4. However, the carbon content (22.5–30 wt%) is relatively high, which, partly as a result, reduces the specific capacity. So far, other organic compounds, such as furalcohol,[14] citric acid,[27] oleic acid,[28] EDTA,[29] ethylene glycol[30] and even ionic liquids[2] have been used as alternative carbon precursors to prepare Fe_3O_4@C composites. As a consequence, the carbon coating layers are usually not strong enough to accommodate the volume expansion, resulting in severe capacity fading and unsatisfactory rate capability.[27,29] Thus far, achieving a uniform carbon coating layer still remains a challenge. Furthermore, the coating carbons derived from the above-mentioned precursors barely contain N species. It has been demonstrated in the literature that N-doping can improve the cycling performance and rate capacity of Fe_3O_4@C composites, for the improvement in electronic conductivity, ion permeability of the carbon layer, charge transfer at the interface and stability of the SEI films.[2,31–35] Thus, it is important to endow the carbon coating with N species to enhance the electrochemical performance of the composites.

Following from the aforementioned studies, the ideal route to fabricate a Fe_3O_4@C composite should have the following features: the coating procedure is high-efficient and tuneable, the coating layer is uniform and continuous, the thickness and surface chemistry of the carbon coating layer are controllable. To fully satisfy these requirements, a novel carbon nanocoating method must be applied, in which the new carbon precursor plays a critical role. Dopamine, a biomolecule that contains catechol and amine functional groups, can self-polymerize at alkaline pH values under oxygen atmosphere. The conformal and continuous polydopamine films can be spontaneously affixed on a hematite surface due to the strong binding affinity of catechol-derivative anchor groups (phenolic hydroxyl) to iron oxide just through immersing the particles into the dopamine solution at 30 °C.[36–38] Taking advantage of the strong and versatile coating capability of this new carbon precursor to iron oxide, it is possible to form a uniform and continuous polydopamine coating layer on the particle surface, which can then be converted into N-doped carbon under heat treatment.[38] Moreover, the thickness of the polydopamine layer can be controlled through varying the initial concentration of dopamine or the polymerization time.[39] Therefore, using dopamine as a precursor has a significant advantage in tuning the compositions and properties of the coating layer, which is essential for material design and optimization. Although dopamine has been previously utilized for the surface modification of various nanoparticles, the use of a dopamine polymer as the N-doped carbon precursor to prepare Fe_3O_4-based anodes for LIBs has not been studied yet. Herein, we take dopamine as a new precursor to obtain N-doped carbon coated nano-sized Fe_3O_4 (Fe_3O_4@NC) composites through a two-step method. This interesting Fe_3O_4@NC composite exhibited outstanding electrochemical performance as a LIB anode with a very high specific capacity of 817 mA h g^{-1} at a current of 500 mA g^{-1} in the initial cycle and a high capacity retention of 99% after 200 cycles.

2 Experimental

2.1 Chemicals

L-Lysine and hexahydrated ferric chloride were obtained from Sigma-Aldrich Corporation. Dopamine hydrochloride was purchased from Beijing Ouhe Technology Co. Ltd. All chemicals were used as received.

2.2 Synthesis of Fe_2O_3 nanoparticles

Uniform rhombic-shaped Fe_2O_3 nanoparticles were prepared according to the method described previously.[40,41] In a typical procedure, 2 mmol of $FeCl_3 \cdot 6H_2O$ and 0.5 mmol of lysine were first dissolved in 100 mL distilled water under vigorous stirring at room temperature for 2 h to form a clear solution. Subsequently, the mixture was transferred to a Teflon-lined stainless steel autoclave of 150 mL capacity, sealed, and maintained at 120 °C for 14 h. Afterwards, the autoclave was allowed to cool down to room temperature. The resulting reddish products were collected by centrifugation and washed three times with distilled water.

2.3 Synthesis of Fe_3O_4@NC composites

Typically, 280 mg hematite particles were dispersed in 50 mL Tris-buffer (pH: ~8.5) by ultrasonication for 30 min to form a suspension. Subsequently, 50 mg dopamine was added to the mixture under stirring. The mixture was subjected to continuous magnetic stirring at 30 °C for 48 h. Afterwards, the precipitates, *i.e.* polydopamine/iron oxide, were collected by centrifugation, then washed three times with deionized water, and then dried at 50 °C in an electric oven for 12 h. The resulting sample was heated in a quartz tube to 150 °C at a rate of 3 °C min^{-1} in Ar atmosphere and kept at this temperature for 1 hour, and then further heated to 500 °C with a heating rate of 5 °C min^{-1}, and kept at this temperature for 4 h. The obtained composite was denoted as Fe_3O_4@NC-1.

In order to tune the coating thickness of the carbon layer, sample Fe_3O_4@NC-2 was retained for 4 h during the dopamine coating process, the rest of the reaction conditions were the same as for sample Fe_3O_4@NC-1. Sample Fe_3O_4@NC-3 was prepared similarly to Fe_3O_4@NC-1, but the initial concentration of dopamine was changed from 1 mg mL^{-1} to 3 mg mL^{-1}.

For comparative purposes, a glucose-derived carbon coated Fe_3O_4 (Fe_3O_4@C) composite was also prepared by hydrothermal reaction in an autoclave. Specifically, 280 mg hematite particles were transferred to a clear solution containing 2.8 g glucose dissolved in 40 mL deionized water. The mixture was ultrasonically dispersed for 20 min and placed in a 50 mL Teflon-sealed autoclave, which was then heated at 180 °C in an electric oven for 6 h. The rest of the process is similar to that used for Fe_3O_4@NC-1.

2.4 Characterization

Thermogravimetric analysis was measured from room temperature to 600 °C in air with a heating rate of 10 °C min^{-1} using a STA449 F3 Jupiter thermogravimetric analyzer (NETZSCH). The X-ray diffraction (XRD) measurements were taken on a Rigaku

D/Max 2400 diffractometer using Cu–K radiation (40 kV, 100 mA, $\lambda = 1.5406$ Å). Scanning electron microscopy (SEM) investigations were carried out with a FEI Nova NanoSEM 450 instrument. Transmission electron microscopy (TEM) analyses were carried out with a Tecnai $G^2$20S-Twin equipment operating at 200 kV. The samples for TEM analysis were prepared by dropping an ethanol droplet of the products on carbon-coated copper grids and drying at room temperature. X-ray photoelectron spectroscopy (XPS) studies were performed using a monochromatic Al Kα radiation (ESCALAB250, thermo VG), and the binding energies of the samples were calibrated by taking the carbon 1s peak as a reference (284.6 eV).

2.5 Electrochemical measurements

Electrochemical experiments were performed *via* CR2025 coin-type test cells assembled in an argon-filled glove box with lithium metal as the counter and reference electrodes at room temperature. The working electrodes were prepared by mixing the Fe_3O_4@NC composites or Fe_3O_4@C, carbon black, and poly(vinyldifluoride) (PVDF) at a weight ratio of 70 : 15 : 15, and pasting the mixture on pure Cu foil. The electrode area was 1.13 cm^2 and the loading of the active material was 2.5–3.0 mg cm^{-2}. A Celgard 2400 membrane was used as a separator. The electrolyte consisted of a solution of 1 M $LiPF_6$ in dimethyl carbonate (DMC), ethyl methyl carbonate (EMC) and ethylene carbonate (EC) (1 : 1 : 1 *v*/*v*/*v*). The discharge–charge measurements were carried out at several different current densities between the cut off potentials of 0.01 and 3 V using a Land CT2001A battery test system. The specific capacity of the Fe_3O_4@NC composites was calculated on the basis of the total mass of Fe_3O_4 and nitrogen-doped carbon. Cyclic voltammogram (CV) measurements and electrochemical impedance spectra (EIS) were performed on a CHI660D electrochemical workstation.

3 Results and discussion

The fabrication process of Fe_3O_4@NC nanocomposites is schematically illustrated in Fig. 1. Initially, the rhombic-shaped hematite (α-Fe_2O_3) nanoparticles, obtained from the hydrothermal method assisted with amino acids, were coated with polydopamine through immersion of the hematite nanoparticles in a dopamine aqueous solution (pH: ~8.5). The general coating mechanism of dopamine on inorganic solid surfaces has been studied previously.[36,42–46] In the present study, catechol-derivative anchor groups showed a strong and irreversible binding affinity to the surface Fe–OH of iron oxides, resulting in the dehydration and formation of a charge-transfer complex. Subsequently, through an oxidization and cyclization reaction, the dopamine monomer translates into 5,6-dihydroxyindole, an important intermediate, which is covalently joined *via* aryl–aryl linkages, giving a conformal and continuous polymer layer.[36,46] Afterwards, the core–shell structure α-Fe_2O_3@polydopamine was transformed into Fe_3O_4@NC nanocomposites by thermal annealing at 500 °C.

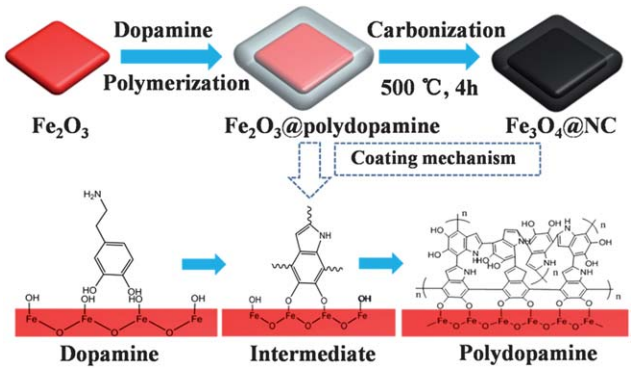

Fig. 1 Schematic illustration of the fabrication of Fe_3O_4@NC composites and the coating mechanism of polydopamine on the surface of an iron oxide nanoparticle.

Fig. 2 shows the powder X-ray diffraction (XRD) pattern of the hydrothermal product sample, in which all peaks are in good agreement with α-Fe_2O_3 (JCPDS no.89-8103, $a = b = 5.020$ Å, $c = 13.719$ Å) with the $R\bar{3}c$ space group (JCPDS no.33-0664).[47] In contrast, the diffraction peaks of the Fe_3O_4@NC-1 composite are similar to pure Fe_3O_4 (JCPDS no.65-3107), indicating that the hematite nanoparticles have been transformed into the face-centered cubic phase of magnetite, due to the carbothermic reduction between the polydopamine-derived carbon and α-Fe_2O_3. The XRD pattern of the Fe_3O_4@NC-1 composite shows the absence of peaks corresponding to graphite, which indicates that the carbon layer is in an amorphous state.[14] The energy-dispersive X-ray spectroscopy (EDX) mapping (Fig. 3a) of the elements in the Fe_3O_4@NC-1 composite shows the concordance of N, C and Fe signals, suggesting the uniform distribution of C and N elements. The high-resolution N1s XPS spectrum of the Fe_3O_4@NC-1 (Fig. 3b) could be identified into two component peaks at the Binding Energy (BE) of 400.2 and 398.5 eV, corresponding to C–N and C=N, respectively,[2,32,48] demonstrating the presence of nitrogen in the structure of the carbon layer. Hence, polydopamine has been transformed into N-doped carbon after pyrolysis. Moreover, the nitrogen content

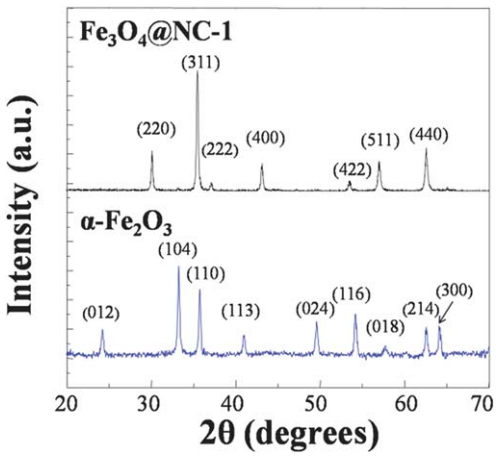

Fig. 2 XRD patterns of Fe_3O_4@NC-1 composite and rhombic-shaped Fe_2O_3.

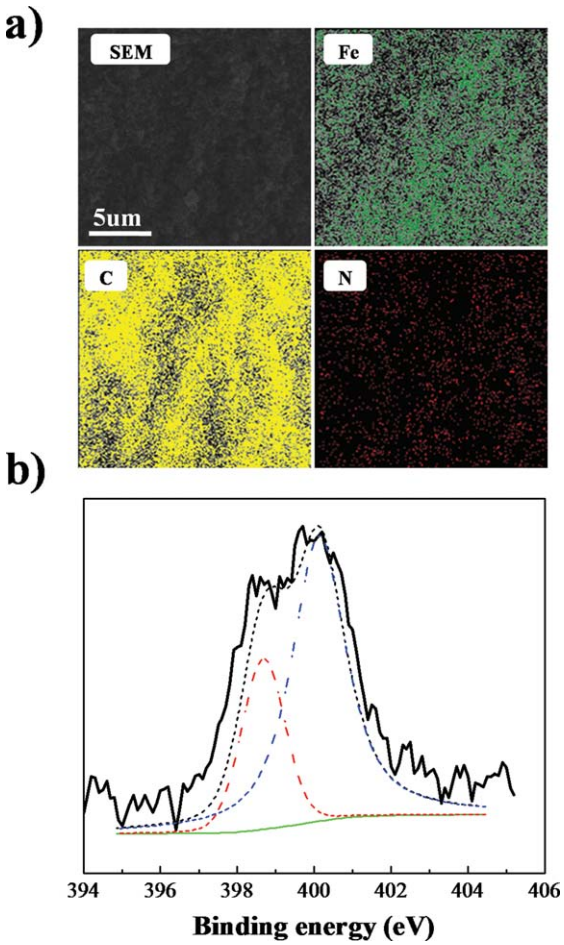

Fig. 3 (a) SEM image and EDX element maps of Fe_3O_4@NC-1 composite, (b) high-resolution N 1s spectra of Fe_3O_4@NC-1 composite.

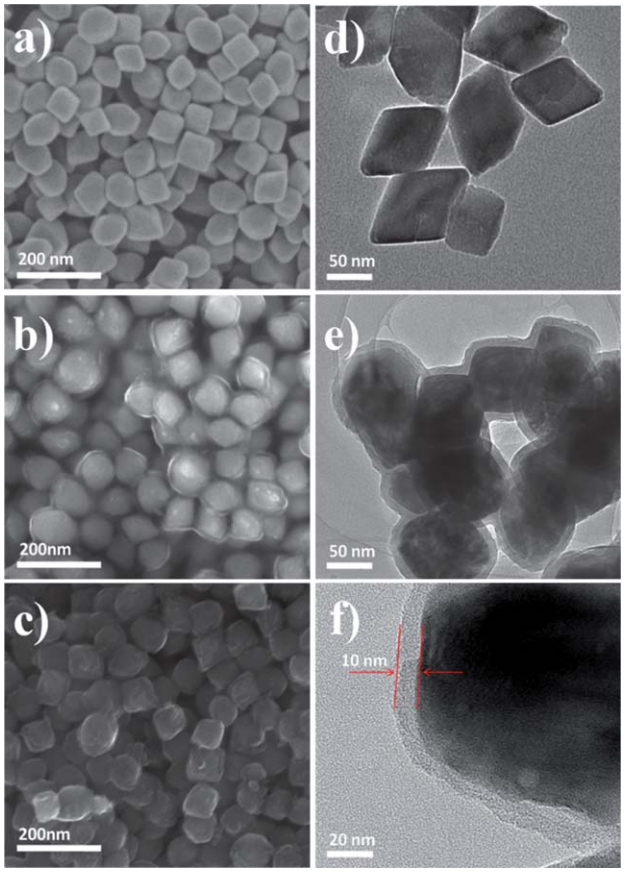

Fig. 4 SEM images of (a) as-synthesized rhombic-shaped hematite, (b) carbon precursor coated hematite, (c) carbon coated rhombic-shaped Fe_3O_4 (Fe_3O_4@NC-1 composite); TEM images of (d) rhombic-shaped hematite, (e) Fe_3O_4@NC-1 composite, and (f) high-magnification image of a Fe_3O_4@NC-1 composite.

on the surface of Fe_3O_4@NC-1 is calculated to be 2.64 wt% according to the X-ray photoelectron spectroscopy.

Fig. 4a shows the scanning electron microscopy (SEM) images of the as-synthesized α-Fe_2O_3 nanoparticles, which consist of uniform rhombic-shaped particles with a center diameter of ~80 nm and length of ~100 nm. A closer examination reveals that the surface of the rhombic particles is very smooth (Fig. 4d). Fig. 4b shows the SEM of the carbon-precursor-coated α-Fe_2O_3. As can be seen from the images, the α-Fe_2O_3 nanoparticles are well-dispersed in the polydopamine shell and both the outer carbon-precursor layer and the inner hematite core are visible. There is no significant change in the morphology of hematite@polydopamine, indicating conformal and uniform coating of polydopamine on the hematite surface. This guarantees the formation of a uniform and continuous carbon layer after thermal treatment.

As can be seen from the SEM (Fig. 4c) and TEM (Fig. 4e) images, the Fe_3O_4@NC-1 composite has the same overall morphology as its α-Fe_2O_3 precursor except for the uniform and continuous carbon coating. In Fig. 4f, the TEM image of Fe_3O_4@NC-1 shows that Fe_3O_4 nanoparticles were coated with a uniform thin carbon layer with a thickness of ~10 nm, displaying a typical core–shell nanostructure.

Based on the hypothesis that the specific capacity mainly comes from the magnetite and the coating carbon only acts as the barrier which makes a much smaller contribution to the specific capacity of the composites, Fe_3O_4@NC composites with different ratios of Fe_3O_4 to N-doped carbon were also prepared in order to determine the optimal composition for electrochemical performance. Fe_3O_4@NC-2 and Fe_3O_4@NC-3 were prepared by varying the coating time and initial dopamine concentration, respectively, yet keeping other preparation variables fixed. The coating time was shortened from 48 to 4 h and the corresponding product denoted as Fe_3O_4@NC-2. We varied the initial dopamine concentration from 1 mg mL^{-1} to 3 mg mL^{-1} and the corresponding product was denoted as Fe_3O_4@NC-3. The carbon content is determined by thermogravimetric analysis. As shown in Fig. 5a, a weight loss below 150 °C is attributed to the evaporation of the adsorbed moisture or gas molecules, and a major weight loss takes place between 300 and 400 °C, giving rise to an observed weight loss of 16 wt%, 3 wt% and 28 wt% for samples Fe_3O_4@NC-1, Fe_3O_4@NC-2, and Fe_3O_4@NC-3, respectively. As seen from the TEM images of Fe_3O_4@NC-2 and Fe_3O_4@NC-3 (Fig. S2†), the two composites both have uniform and continuous carbon coating layers, which are about 2 and 24 nm in thickness, respectively. This indicates that the thickness of the N-doped carbon layer can be tailored

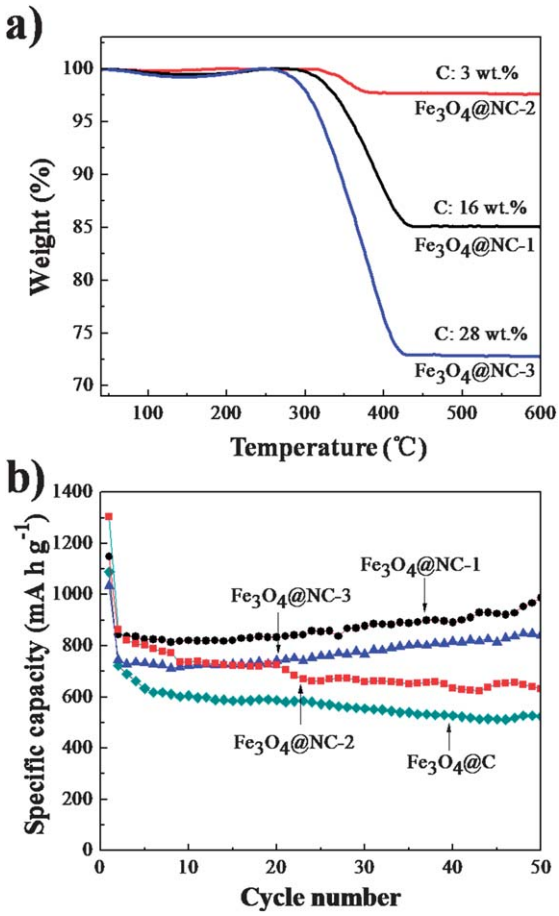

Fig. 5 (a) TG curves of Fe_3O_4@NC composites with different carbon content, and (b) discharge capacity *versus* cycle number plots of Fe_3O_4@NC composites and Fe_3O_4@C measured at a current density of 500 mA g^{-1}.

through varying the experimental conditions while maintaining uniformity and continuity. The cycling performances of Fe_3O_4@NC-1, Fe_3O_4@NC-2, Fe_3O_4@NC-3, and, for comparison, Fe_3O_4@C (the carbon content is 31 wt% and the thickness of the carbon shell is ~25 nm, which are shown in Fig. S3†) are compared in Fig. 5b. It is clear that the capacity fading of Fe_3O_4@C is rather severe at a current density of 500 mA g^{-1}, and the capacity after 50 cycles declines to only 524 mA h g^{-1}, which is owing to the lackluster electron conductivity and ion permeability of the glucose derived carbon shell at relative high current density, however, its electrochemical performance is still superior to the pure Fe_3O_4 nanoparticles (Fig. S5a†) which lack the protective effect of the carbon shell. As for the Fe_3O_4@NC-2 composite, although capacity fading is substantially subdued as compared to Fe_3O_4@C, this sample still maintains only 632 mA h g^{-1} (72.6% of the second cycle capacity) after 50 cycles. The Fe_3O_4@NC-1 composite with a carbon content of 16 wt%, on the other hand, experiences a negligible capacity decrease from the 2nd cycle onwards. Consequently, a capacity as high as 976 mA h g^{-1} (117.2% of the second cycle capacity) was sustainable for 50 cycles. In the case of sample Fe_3O_4@NC-3, there is also negligible capacity loss during cycling, despite the initial capacity or the fiftieth cycle capacity (only 739 and 828 mA h g^{-1}, respectively) being relatively low compared to that of Fe_3O_4@NC-1. This is attributed to the increased weight percentage of the inactive carbon coatings in the composite. Interestingly, the capacities of the Fe_3O_4@NC-1 and Fe_3O_4@NC-3 nanocomposites increased gradually, which can be ascribed to the activation of the active materials and the growth of a polymer/gel like film caused by the decomposition of the electrolyte. As is known, the activation process decreases cell resistance, and the *in situ* generated polymer/gel like film ensures mechanical cohesion and delivers excess capacity at low potential through a so-called "pseudo-capacitance-type behavior".[49–53] The electrochemical performance of the Fe_3O_4@NC composites confirms our hypothesis, mentioned above, that a low carbon percentage results in capacity fading, whereas high carbon percentage leads to reduced capacity. Therefore, the ratio of carbon coating to Fe_3O_4 has to be optimized to balance the concurrent need for high capacity and good cyclability. According to this consideration, sample Fe_3O_4@NC-1 would be a candidate to achieve a balance between the specific capacity and cycle stability, which was subsequently taken as the delegate to evaluate the electrochemical performance of Fe_3O_4@NC in detail.

Discharge–charge cycling was carried out in the voltage range of 0.01–3.0 V (*vs.* Li) at a current density of 500 mA g^{-1} for up to 50 cycles. Fig. 6a depicts the discharge–charge voltage profiles of the Fe_3O_4@NC-1 composite for the first, second, fifth, tenth and fiftieth cycles. The sample shows a very high first-cycle discharge capacity of 1173 mA h g^{-1} and delivers a corresponding charge capacity of 817 mA h g^{-1}, giving rise to an irreversible capacity loss of ~30.3%. The irreversible capacity loss of ~30.3% may be mainly attributed to irreversible processes such as inevitable formation of a solid electrolyte interface (SEI layer) and electrolyte decomposition, which are common to most anode materials. Moreover, the relative low carbonization temperature results in the abundant oxygen-containing functional groups, which will exacerbate the irreversible capacity losses. However, on the other hand, with the increase of the pyrolysis temperatures, the electrochemical performances of the composites declined significantly, as shown in Fig. S4.† Based on the above consideration, in this study we selected a pyrolysis temperature of 500 °C. From the second cycle onwards, Fe_3O_4@NC-1 exhibits very high capacities of over 800 mA h g^{-1} with a stable capacity retention of above 100% for over 50 cycles. Cyclic voltammetry (CV) was also carried out to understand the reactive process. Li metal was used for the counter and reference electrodes. Fig. 6b shows the first three CV curves of Fe_3O_4@NC-1 at room temperature in the range of 0.01–3.0 V at a slow scan rate of 0.5 mV s^{-1}. In the first cycle, a dominant pair of redox peaks can be clearly identified at ~0.5 and 1.75 V, during the cathodic and anodic sweep, respectively. The broad peak at 0.50 V in the cathodic process can be associated with the reduction of Fe^{3+} and Fe^{2+} to Fe^0 and the irreversible reaction related to the decomposition of the electrolyte combined with the formation of SEI films. The anodic peak present at 1.75 V represents the reversible oxidation of Fe^0 to Fe^{2+} and Fe^{3+}. In the subsequent cycles, the cathodic and anodic peak potentials shift to 0.72 and 1.9 V,

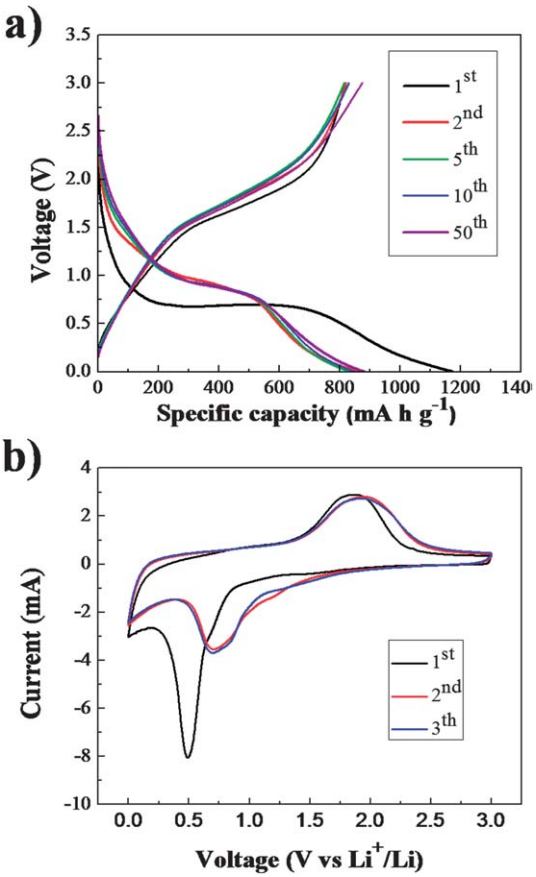

Fig. 6 (a) Discharge–charge profiles of the Fe_3O_4@NC-1 nanocomposite for the initial 50 cycles at a current density of 500 mA g^{-1}; and (b) cyclic voltammograms at a scan rate of 0.5 mV s^{-1} between 0.01 and 3.0 V, all potentials are with reference to Li$^+$/Li.

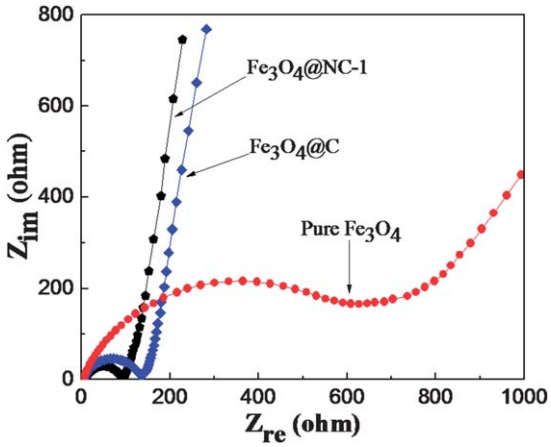

Fig. 7 Nyquist plots of the electrodes composed of Fe_3O_4@NC-1, Fe_3O_4@C and pure Fe_3O_4.

respectively. As for the cathodic process, both the peak current and the integrated area decrease in the second cycle, indicating the occurrence of an irreversible process for the electrode material. However, there is no obvious potential change in the anodic peak, suggesting that the electrochemical reaction has proceeded to an identical extent. The CV curves of the Fe_3O_4@NC-1 composite electrode are stable and show good reversibility after the second cycle, which is consistent with its good cycling performance as discussed before. Distinctly, the lithium storage mechanism of the Fe_3O_4@CN-1 composite is similar to other iron oxide based electrodes, exhibiting the pattern that is consistent with previously reported data.[11,12,54–56] However, due to the presence of a conductive N-doped carbon layer, the Fe_3O_4@NC-1 composite exhibits much lower resistance than the Fe_3O_4 nanoparticles and Fe_3O_4@C composite as evidenced by the drastically reduced diameter of the semicircle at the high-frequency region and the appreciably steep slope line at the low-frequency region in the electrochemical impedance spectroscopy (EIS) patterns (Fig. 7), which is attributed to the unique N-doped carbon shell derived from polydopamine. The results of the EIS also confirm the hypothesis that nitrogen-doping can improve the electron conductivity and ion permeability of the carbon shell and the charge transfer at the interface. The rate performance and the cycling stability during the lithium-ion insertion/extraction processes are key factors for successful practical application as anode electrodes. Herein, the rate capability of Fe_3O_4@NC-1 was evaluated at various currents in the range of 500–5000 mA g^{-1} at a cut-off voltage between 0.01 and 3.0 V Li$^+$/Li, and the results are given in Fig. 8a. The discharge capacities are retained at 803, 595 and 396 mA h g^{-1} at the current of 500, 1000 and 2000 mA g^{-1}, respectively. The capacities at a higher current of 5000 mA g^{-1}, although fading rapidly, can still deliver 85 mA h g^{-1}. Moreover, when the current is restored to 500 mA h g^{-1} after 60 cycles, Fe_3O_4@NC-1 still delivers 840 mA h g^{-1}, which is ~100.8% of the initial capacity. Compared with the Fe_3O_4@NC-1 composite, the rate performance of bare Fe_3O_4 particles is lacklustre (Fig. S5b†), especially at high rate, for example, when the current is higher than 2000 mA g^{-1}, Fe_3O_4 particles have nearly no capacity. This phenomenon can be attributed to the severe aggregation of the nanoparticles, pulverization of the electrode and the low electronic conductivity and ion permeability without carbon protection. In comparison with the recent reports on iron oxide based anode materials, the Fe_3O_4@NC-1 composite shows outstanding rate capability and good cycle stability (for details, see Table S1†). This remarkably improved electrochemical performance can undoubtedly be attributed to the homogeneous and appropriate N-doped carbon coating layer, which not only acts as a barrier to prevent aggregation of the nanoparticles and pulverization of the electrode, but also provides rapid electron transport network and maintains the structure integrity. To examine whether sample Fe_3O_4@NC-1 has an excellent cycling stability, we prolonged the cycle number up to 200, and the cycling performance of this electrode is shown in Fig. 8b. No capacity decay was detected after 100 cycles, capacity retention after 200 cycles was 99%, although we changed the current to 1000 mA g^{-1} from cycle number of 100. Moreover, it can be seen that all the discharge curves are almost overlapping with the charge curves with a Coulombic efficiency above 98%. Combining the high reversible capacity, high Coulombic efficiency, stable cycle performance, and the

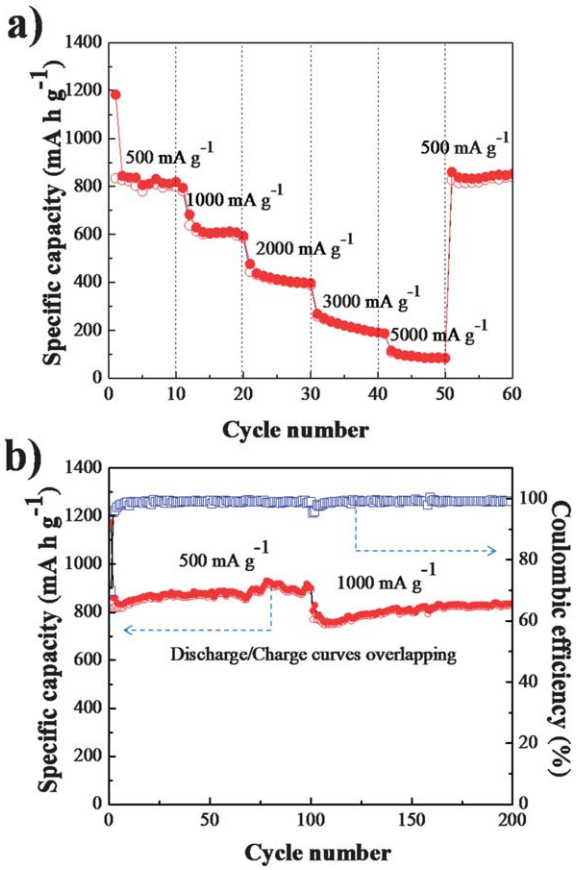

Fig. 8 (a) The rate capability of Fe_3O_4@NC-1 at different current densities and (b) long-term cycling of Fe_3O_4@NC-1. The solid and hollow symbols represent discharge and charge capacities, respectively.

outstanding rate capability, we conclude that this Fe_3O_4@NC-1 composite is a promising candidate as an anode material for LIBs.

In addition, we have extended this method to the preparation of polydopamine coated spindle shaped-Fe_2O_3 and rod shaped-β-FeOOH. As shown in the SEM images (Fig. S6†), the coating was successful and the coating method may be applied to other metal oxides.

4 Conclusions

We have demonstrated that dopamine can be used as a new nitrogen-containing carbon precursor for the fabrication of high performance iron oxide-based lithium ion battery anodes. In this study, uniform and continuous carbon coated iron oxide composites could be obtained by simple immersion of α-Fe_2O_3 in a dopamine aqueous solution, followed by subsequent carbonization. Thanks to the unique characteristics of this new carbon precursor, we could easily tailor the thickness of the carbon layer while maintaining its uniformity and continuity, which allows a balance between the specific capacity and cycling stability. Moreover, the polydopamine derived carbon contains N species which can enhance the electrochemical performance of the composite electrode. As a consequence, the resulting material with a 10 nm thickness of uniform N-doped carbon coating layer exhibits high specific capacity, superior rate capability and excellent cycling performance for LIBs. This synthetic approach is relatively simple, yet very effective, and owing to its versatility it can also be extended to modify other electrode materials for electrochemical devices.

Acknowledgements

The project was supported by the Fundamental Research Funds for the Central Universities (DUT12ZD218), the Program for New Century Excellent Talents in University of China (NCET-08-0075), and the PhD Programs Foundation (20100041110017) of the Ministry of Education of China.

Notes and references

1 C. M. Ban, Z. C. Wu, D. T. Gillaspie, L. Chen, Y. F. Yan, J. L. Blackburn and A. C. Dillon, *Adv. Mater.*, 2010, **22**, 145.
2 Y. Ma, C. Zhang, G. Ji and J. Y. Lee, *J. Mater. Chem.*, 2012, **22**, 7845.
3 Y. D. Huang, Z. F. Dong, D. Z. Jia, Z. P. Guo and W. Choe, *Electrochim. Acta*, 2011, **56**, 9233.
4 S. L. Chou, J. Z. Wang, D. Wexler, K. Konstantinov, C. Zhong, H. K. Liu and S. X. Dou, *J. Mater. Chem.*, 2010, **20**, 2092.
5 J. S. Chen, L. A. Archer and X. W. Lou, *J. Mater. Chem.*, 2011, **21**, 9912.
6 P. L. Taberna, S. M. P. Poizot, P. Simon and J. M. Tarascon, *Nat. Mater.*, 2006, **5**, 567.
7 W. M. Zhang, X. L. Wu, J. S. Hu, Y. G. Guo and L. J. Wan, *Adv. Funct. Mater.*, 2008, **18**, 3941.
8 J. S. Zhou, H. H. Song, X. H. Chen, L. J. Zhi, S. B. Yang, J. P. Huo and W. T. Yang, *Chem. Mater.*, 2009, **21**, 2935.
9 Z. M. Cui, L. Y. Jiang, W. G. Song and Y. G. Guo, *Chem. Mater.*, 2009, **21**, 1162.
10 G. M. Zhou, D. W. Wang, F. Li, L. L. Zhang, N. Li, Z. S. Wu, L. Wen, G. Q. Lu and H. M. Cheng, *Chem. Mater.*, 2010, **22**, 5306.
11 M. Zhang, D. N. Lei, X. M. Yin, L. B. Chen, Q. H. Li, Y. G. Wang and T. H. Wang, *J. Mater. Chem.*, 2010, **20**, 5538.
12 S. Q. Wang, J. Y. Zhang and C. H. Chen, *J. Power Sources*, 2010, **195**, 5379.
13 J. Z. Wang, C. Zhong, D. Wexler, N. H. Idris, Z. X. Wang, L. Q. Chen and H. K. Liu, *Chem.–Eur. J.*, 2011, **17**, 661.
14 Y. Z. Piao, H. S. Kim, Y. E. Sung and T. Hyeon, *Chem. Commun.*, 2010, **46**, 118.
15 T. Yoon, C. Chae, Y. K. Sun, X. Zhao, H. H. Kungc and J. K. Lee, *J. Mater. Chem.*, 2011, **21**, 17325.
16 E. Kang, Y. S. Jung, A. S. Cavanagh, G. H. Kim, S. M. George, A. C. Dillon, J. K. Kim and J. Lee, *Adv. Funct. Mater.*, 2011, **21**, 2430.
17 T. Zhu, J. S. Chen and X. W. Lou, *J. Phys. Chem. C*, 2011, **115**, 9814.
18 S. M. Yuan, J. X. Li, L. T. Yang, L. W. Su, L. Liu and Z. Zhou, *ACS Appl. Mater. Interfaces*, 2011, **3**, 705.
19 J. S. Chen, Y. M. Zhang and X. W. Lou, *ACS Appl. Mater. Interfaces*, 2011, **3**, 3276.

20 Y. Zhu, Y. J. Bai, F. D. Han, Y. X. Qi, N. Lun, B. Yao and J. X. Zhang, *Mater. Lett.*, 2011, **65**, 3157.
21 F. Cheng, K. L. Huang, S. Q. Liu, J. L. Liu and R. J. Deng, *Electrochim. Acta*, 2011, **56**, 559.
22 J. Hu, H. Li, X. Huang and L. Chen, *Solid State Ionics*, 2006, **177**, 2791.
23 J. Jamnik and J. Maier, *Phys. Chem. Chem. Phys.*, 2003, **5**, 5215.
24 X. Zhang, Z. Xing, L. L. Wang, Y. C. Zhu, Q. W. Li, J. W. Liang, Y. Yu, T. Huang, K. B. Tang, Y. T. Qian and X. Y. Shen, *J. Mater. Chem.*, 2012, **22**, 17864.
25 S. M. Yuan, Z. Zhou and G. Li, *CrystEngComm*, 2011, **13**, 4709.
26 T. Muraliganth, A. V. Murugan and A. Manthiram, *Chem. Commun.*, 2009, 7360.
27 H. Liu, G. X. Wang, J. Z. Wang and D. Wexler, *Electrochem. Commun.*, 2008, **10**, 1879.
28 F. Cheng, K. L. Huang, S. Q. Liu, J. L. Liu and R. J. Deng, *Electrochim. Acta*, 2011, **56**, 5593.
29 J. C. Zhang, W. Q. Shen, Z. W. Zhang, D. Y. Pan and M. H. Wu, *Mater. Lett.*, 2010, **64**, 817.
30 Q. M. Zhang, Z. C. Shi, Y. F. Deng, J. Zheng, G. C. Liu and G. H. Chen, *J. Power Sources*, 2012, **197**, 305.
31 A. L. M. Reddy, A. Srivastava, S. R. Gowda, H. Gullapalli, M. Dubey and P. M. Ajayan, *ACS Nano*, 2010, **4**, 6337.
32 L. Zhao, Y. S. Hu, H. Li, Z. X. Wang and L. Q. Chen, *Adv. Mater.*, 2011, **23**, 1385.
33 H. Jiang, L. P. Yang, C. Z. Li, C. Y. Yan, P. S. Lee and J. Mab, *Energy Environ. Sci.*, 2011, **4**, 1813.
34 X. R. Wang, X. L. Li, L. Zhang, Y. K. Yoon, P. K. Weber, H. L. Wang, J. Guo and H. J. Dai, *Science*, 2009, **324**, 768.
35 A. L. M. Reddy, A. Srivastava, S. R. Gowda, H. Gullapalli, M. Dubey and P. M. Ajayan, *ACS Nano*, 2010, **4**, 6337.
36 H. Lee, S. M. Dellatore, W. M. Miller and P. B. Messersmith, *Science*, 2007, **318**, 426.
37 Y. H. Lee, H. Lee, Y. B. Kim, J. Kim, T. Hyeon, H. W. Park, P. B. Messersmith and T. G. Park, *Adv. Mater.*, 2008, **20**, 4154.
38 R. Liu, S. M. Mahurin, C. Li, R. R. Unocic, J. C. Idrobo, H. J. Gao, S. J. Pennycook and S. Dai, *Angew. Chem., Int. Ed.*, 2011, **50**, 6799.
39 N. Liu, H. Wu, M. T. McDowell, Y. Yao, C. M. Wang and Y. Cui, *Nano Lett.*, 2012, **12**, 3315.
40 G. H. Wang, W. C. Li, K. M. Jia, B. Spliethoff, F. Schüth and A. H. Lu, *Appl. Catal., A*, 2009, **364**, 42.
41 G. H. Wang, W. C. Li, K. M. Jia, A. H. Lu, M. Feyen, B. Spliethoff and F. Schüth, *Nano*, 2011, **6**, 469.
42 E. Amstad, A. U. Gehring, H. Fischer, V. V. Nagaiyanallur, G. Hähner, M. Textor and E. Reimhult, *J. Phys. Chem. C*, 2011, **115**, 683.
43 N. H. Andersen, T. E. Mates, M. S. Toprak, G. D. Stucky, F. W. Zok and J. H. Waite, *Langmuir*, 2009, **26**, 3323.
44 M. J. Harrington, A. Masic, N. H. Andersen, J. H. Waite and P. Fratzl, *Science*, 2010, **328**, 216.
45 D. R. Dreyer, D. J. Miller, B. D. Freeman, D. R. Paul and C. W. Bielawski, *Langmuir*, 2012, **28**, 6428.
46 S. Hong, K. Y. Kim, H. J. Wook, S. Y. Park, K. D. Lee, D. Y. Lee and H. Lee, *Nanomedicine*, 2011, **6**, 793.
47 J. S. Chen, T. Zhu, X. H. Yang, H. G. Yang and X. W. Lou, *J. Am. Chem. Soc.*, 2010, **132**, 13162.
48 H. Schmiers, J. Friebel, P. Streubel, R. Hesse and R. Kopsel, *Carbon*, 1999, **37**, 1965.
49 C. T. Cherian, J. Sundaramurthy, M. Kalaivani, P. Ragupathy, P. S. Kumar, V. Thavasi, M. V. Reddy, C. H. Sow, S. G. Mhaisalkar, S. Ramakrishna and B. V. R. Chowdari, *J. Mater. Chem.*, 2012, **22**, 12198.
50 S. Laruelle, S. Grugeon, P. Poizot, M. Dollé, L. Dupont and J. M. Tarascon, *J. Electrochem. Soc.*, 2002, **149**, 627.
51 G. Zhou, D. W. Wang, F. Li, L. Zhang, N. Li, Z. S. Wu, L. Wen, G. Q. Lu and H. M. Cheng, *Chem. Mater.*, 2010, **22**, 5306.
52 F. Han, W. C. Li, M. R. Li and A. H. Lu, *J. Mater. Chem.*, 2012, **22**, 9645.
53 Z. Y. Wang, D. Y. Luan, S. Madhavi, Y. Hu and X. W. Lou, *Energy Environ. Sci.*, 2012, **5**, 5252.
54 J. X. Li, Y. Zhao, Y. H. Ding and L. H. Guan, *RSC Adv.*, 2012, **2**, 4205.
55 B. Wang, J. S. Chen and X. W. Lou, *J. Mater. Chem.*, 2012, **22**, 3315.
56 Z. Y. Wang, D. Y. Luan, S. Madhavi, C. M. Li and X. W. Lou, *Chem. Commun.*, 2011, **47**, 8061.